JOURNAL OF GEOPHYSICAL RESEARCH, VOL. 109, B12310, doi:10.1029/2004JB003031, 2004

Stress interaction between subduction earthquakes and forearc strike-slip faults: Modeling and application to the northern Caribbean plate boundary

Uri ten Brink
U.S. Geological Survey, Woods Hole, Massachusetts, USA

Jian Lin
Department of Geology and Geophysics, Woods Hole Oceanographic Institution, Woods Hole, Massachusetts, USA

Received 19 February 2004; revised 22 July 2004; accepted 1 October 2004; published 24 December 2004.

[1] Strike-slip faults in the forearc region of a subduction zone often present significant seismic hazard because of their proximity to population centers. We explore the interaction between thrust events on the subduction interface and strike-slip faults within the forearc region using three-dimensional models of static Coulomb stress change. Model results reveal that subduction earthquakes with slip vectors subparallel to the trench axis enhance the Coulomb stress on strike-slip faults adjacent to the trench but reduce the stress on faults farther back in the forearc region. In contrast, subduction events with slip vectors perpendicular to the trench axis enhance the Coulomb stress on strike-slip faults farther back in the forearc, while reducing the stress adjacent to the trench. A significant contribution to Coulomb stress increase on strike-slip faults in the back region of the forearc comes from "unclamping" of the fault, i.e., reduction in normal stress due to thrust motion on the subduction interface. We argue that although Coulomb stress changes from individual subduction earthquakes are ephemeral, their cumulative effects on the pattern of lithosphere deformation in the forearc region are significant. We use the Coulomb stress models to explain the contrasting deformation pattern between two adjacent segments of the Caribbean subduction zone. Subduction earthquakes with slip vectors nearly perpendicular to the Caribbean trench axis is dominant in the Hispaniola segment, where the strike-slip faults are more than 60 km inland from the trench. In contrast, subduction slip motion is nearly parallel to the Caribbean trench axis along the Puerto Rico segment, where the strike-slip fault is less than 15 km from the trench. This observed jump from a strike-slip fault close to the trench axis in the Puerto Rico segment to the inland faults in Hispaniola is explained by different distributions of Coulomb stress in the forearc region of the two segments, as a result of the change from the nearly trench parallel slip on the Puerto Rico subduction interface to the more perpendicular subduction slip beneath Hispaniola. The observations and modeling suggest that subduction-induced strike-slip seismic hazard to Puerto Rico may be smaller than previously assumed but the hazard to Hispaniola remains high. *INDEX TERMS:* 8164 Tectonophysics: Stresses—crust and lithosphere; 7230 Seismology: Seismicity and seismotectonics; 7223 Seismology: Seismic hazard assessment and prediction; 8010 Structural Geology: Fractures and faults; 8123 Tectonophysics: Dynamics, seismotectonics; *KEYWORDS:* stress interaction, subduction, strike-slip faults, forearc, Puerto Rico, Hispaniola

Citation: ten Brink, U., and J. Lin (2004), Stress interaction between subduction earthquakes and forearc strike-slip faults: Modeling and application to the northern Caribbean plate boundary, *J. Geophys. Res.*, *109*, B12310, doi:10.1029/2004JB003031.

1. Introduction

[2] Deformation of the forearc region above subduction zones is impacted by the subduction process. The subduction interface accumulates stress as a result of relative plate motion, and the stress is partially released in finite regions of the interface during earthquakes [e.g., *Wang et al.*, 2003]. The forearc region of the overlying plate is made of heterogeneous lithosphere, whose strength and cohesion are generally lower than those of the subducting lithosphere. Thus, in many cases the forearc region is pervasively deformed, often by earthquakes. Earthquakes that occur within the forearc region could be more

0148-0227/04/2004JB003031$09.00

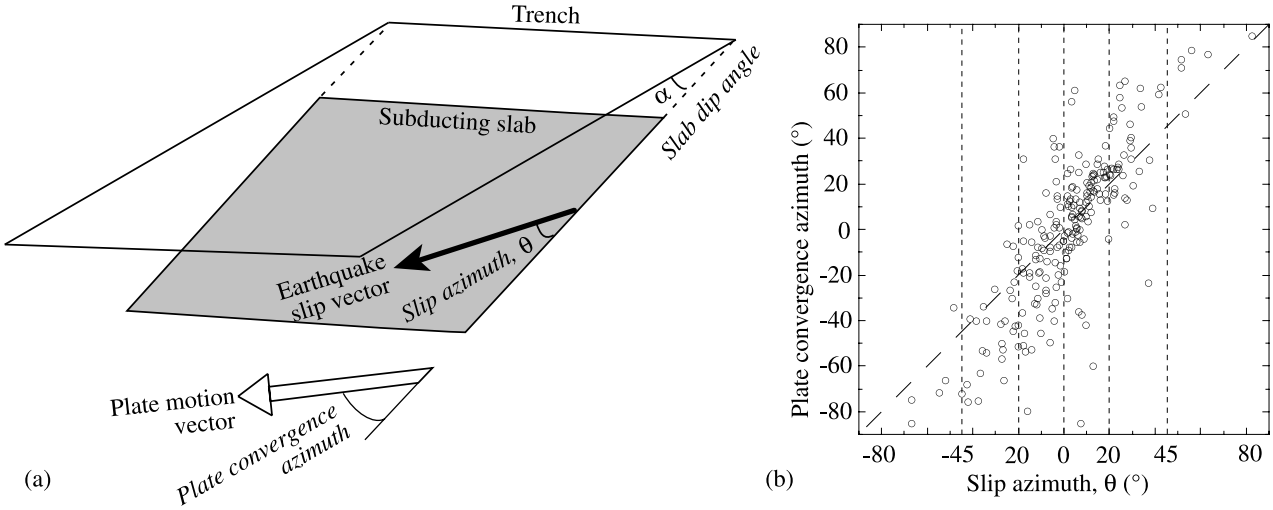

Figure 1. (a) Schematic drawing of slip azimuth (θ) on a patch of the subducting slab. (b) Plate convergence azimuth plotted against slip azimuth (θ) from GPS and large earthquakes for segments of subduction zones around the world. Long dashed line delineates slip azimuth being equal to convergence azimuth. Error bars were omitted for clarity. Data are from *McCaffrey* [1994].

destructive than the often larger earthquakes on the subduction interface because of their shallow depth and proximity to population centers as exemplified by the 1995 Kobe earthquake.

[3] Plate convergence at subduction zones and the slip vector of thrust earthquakes are often oblique to, rather than perpendicular to, the trench axis. Oblique subduction is qualitatively related to internal forearc deformation in the form of strike-slip faults, block rotation, and along-arc extension or compression, which are necessary to compensate for geometrical changes in space due to the arcuate shape of some arcs [e.g., *Geist and Scholl*, 1992]. Because the slip direction of subduction earthquakes is often more perpendicular to the trench axis than that of the plate convergence direction (Figure 1b), the difference between the plate convergence vector and the slip vector of subduction earthquakes was proposed to be accommodated by slip on strike-slip faults in the forearc that are parallel to the trench axis [e.g., *McCaffrey*, 1994]. The difference between the convergence and slip vectors is thought to depend on the balance of shear forces between the subduction interface and the strike-slip faults within the forearc [*Fitch*, 1972; *Beck*, 1983; *McCaffrey*, 1993, 1994].

[4] *Savage* [1983] has investigated the stress relationship between subduction and upper plate deformation using analytical elastic dislocation solutions, and *Taylor et al.* [1998] have used three-dimensional (3-D) elastic finite element models to study the static stress transfer of the subducting plates to the arc and back-arc regions. Various studies have illustrated that strike-slip faults can interact through static stress transfer not only with nearly strike-slip faults [e.g., *Stein*, 1999] but also with neighboring thrust fault systems [e.g., *Kurushin et al.*, 1997; *Lin and Stein* [2004]. Using examples in the Los Angeles region in southern California, *Anderson et al.* [2003] further proposed that strike-slip and thrust faults may interact through both static and dynamic stress changes associated with earthquakes.

[5] Here we present generic models showing how thrust earthquakes on a subducting plate may cause stress changes along strike-slip faults in the overlying forearc region. Using a 3-D boundary element modeling approach [*Toda and Stein*, 2002], we determine the dependence of the calculated stress changes along the forearc strike-slip faults as a function of the slip azimuth of the subduction earthquakes (with respect to the normal to the trench axis) and the coefficient of friction of the forearc faults. Our model results predict that different regions of the forearc may undergo significant stress changes even in cases where the slip direction of a subduction earthquake is perpendicular to the trench axis. The model results also predict that both shear stress and normal stress changes caused by subduction quakes are likely to play a significant role in the slip of forearc strike-slip faults. We use the insight from these stress analyses to explain the observed contrasting styles of forearc deformation between the Puerto Rico and Hispaniola segments of the Caribbean trench, where the North American plate subducts under the Caribbean plate. These model results, together with the observed seafloor deformation and the published earthquake focal mechanisms and GPS observations, help us also to evaluate the seismic hazard of the Puerto Rico and Hispaniola regions.

2. Stress Transferred From a Subduction Earthquake to the Forearc Strike-Slip Faults

[6] We consider stress changes on a left-lateral strike-slip fault (receiver fault) that is parallel to the trench axis, caused by an earthquake (source fault) on the subduction interface. The change in the Coulomb stress on the strike-slip receiver fault is described by $\Delta\sigma_c = \Delta\tau_s + \mu\Delta\sigma_n$, where $\Delta\tau_s$ is the change in shear stress on the receiver fault, μ is the apparent coefficient of friction after compensating the pore fluid effect, and $\Delta\sigma_n$ is the change in stress normal to the receiver fault [e.g., *King et al.*, 1994]. Shear stress change that facilitates sliding is defined as positive. Positive normal

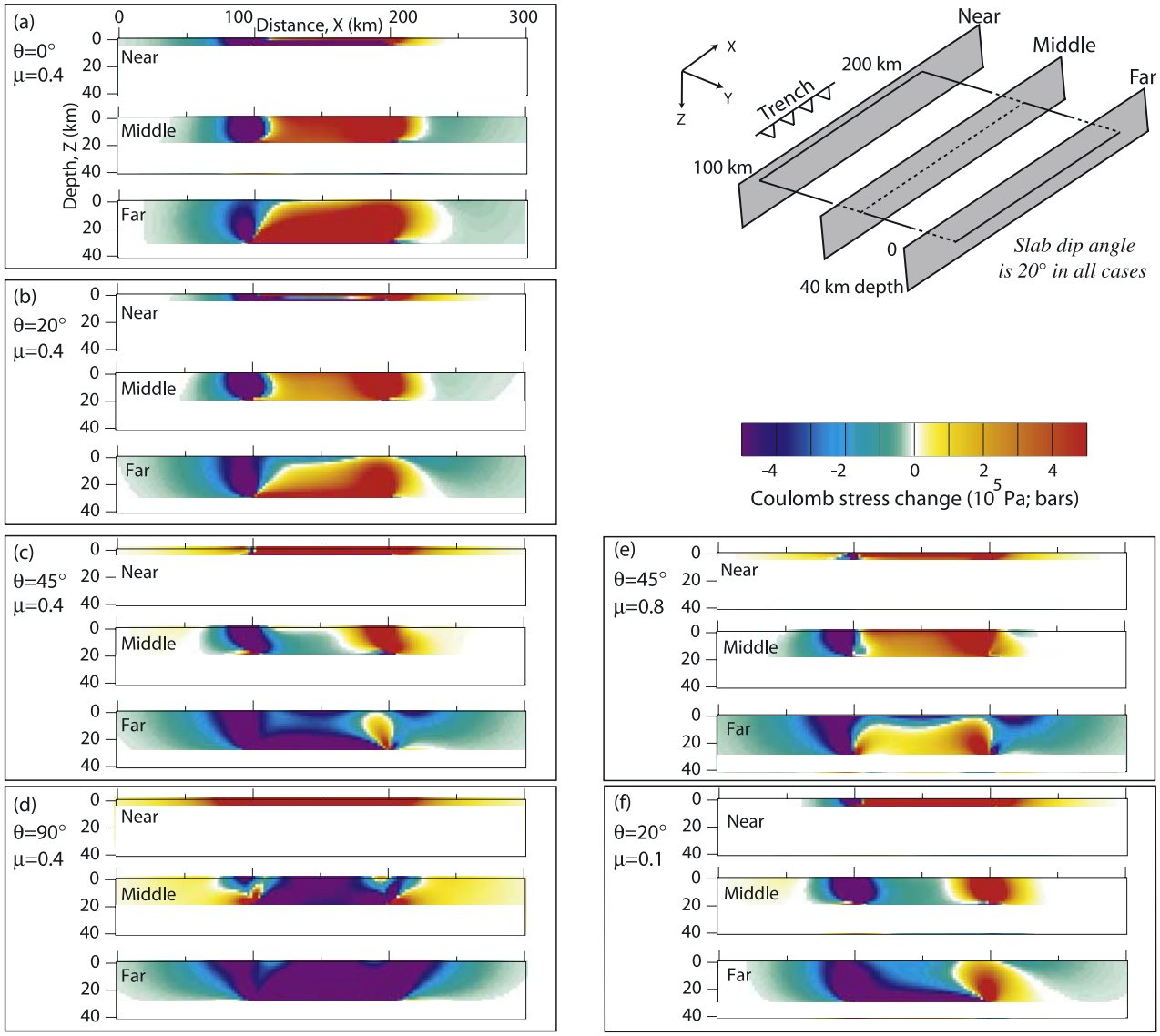

Figure 2. Coulomb stress changes on left-lateral strike-slip fault planes oriented parallel to the trench due to slip on a patch of the subduction interface. (top right) Model geometry and coordinate system. (a–d) Stress changes along fault planes intersecting the patch near, middle, and far from the trench, for different slip orientations ($\theta = 0°$, 20°, 45°, and 90°) calculated with a coefficient of friction $\mu = 0.4$. Only the portion of the fault plane above the subduction patch is shown. This portion represents strike-slip fault planes in the forearc. (e) Same as Figure 2c but with $\mu = 0.8$. (f) Same as Figure 2b but with $\mu = 0.1$. Note the similarity in the pattern of Coulomb stress change between Figures 2b and 2e and between Figures 2c and 2f.

stress change (tension) increases the ability of the strike-slip fault to slide because the fault plane is unclamped.

[7] A global compilation of slip vectors of subduction earthquakes shows that the slip angle with respect to the normal to the trench axis is $\theta < 20°$ for two third of the subduction events and $\theta < 45°$ for 95% of the subduction events (Figure 1). We therefore explore a range of subduction earthquake models that vary from pure thrust perpendicular to the trench axis ($\theta = 0°$), to oblique left-lateral thrust ($20° < \theta < 45°$), and to left-lateral shear parallel to the trench axis ($\theta = 90°$). The subduction interface is represented by a 100 km long ($100 \leq x \leq 200$ km, in Figure 2) and 73 km wide patch that is dipping at 20° and is located at the depth of 5 to 30 km. The Coulomb stress changes induced by the subduction quake on three strike-slip fault planes are illustrated in Figure 2, one intersecting the bottom end of the subduction quake patch (at 82.5 km from the trench), one intersecting the top end of the patch (at 13.8 km from the trench), and one intersecting the middle of the patch (at 50 km from the trench). Although we model the induced stress changes on left-lateral faults in response to a left oblique subduction earthquake, the results are the same for right-lateral strike-slip fault planes in response to a right oblique subduction quake.

[8] Static Coulomb stress changes along left-lateral strike-slip faults intersecting the top end (near the trench),

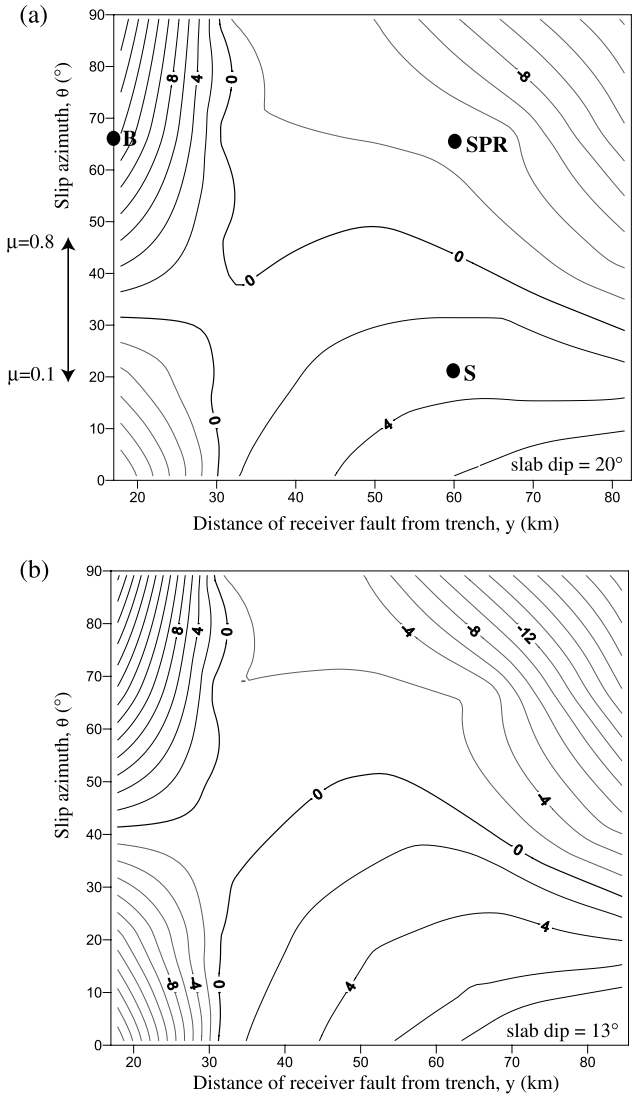

Figure 3. Contours of the average Coulomb stress change ($\Delta\sigma_c$) on a strike-slip fault in the forearc as a function of subduction slip azimuth, θ, and the distance, y, of the fault from the trench. The subduction patch is dipping at 20°. The corresponding parameters for the Puerto Rico/Bunce Fault (B), Hispaniola/Septentrional Fault (S), and SPRFZ (SPR) are also shown. (b) Same as Figure 3 except for a patch dipping at 13°. The stress change was averaged on the part of the fault plane which is between x = 102 km and x = 198 km and between z = 0 and the intersecting depth of the fault with the slipping subduction patch. Figures 3a and 3b show a bimodal distribution of stress change pattern. At low θ, Coulomb stress increases far from the trench and decreases near the trench. At high θ, Coulomb stress decreases far from the trench and increases near the trench. The slip azimuth, θ, at which the modes switch, depends on the coefficient of friction μ.

the middle, and the lower end of the thrust (far from the trench) are shown in Figures 2a–2d. An abrupt change in static stress from negative to positive or vice versa at the top and bottom fault planes occurs at the depths in which the subduction patch intersects these strike-slip fault planes (5 km in the top fault and 30 km in the bottom fault). We limit our discussion to stress changes above the intersections with the subducting patch, which is the region occupied by the forearc. There are additional stress concentrations at the edges of the subducting fault (near x = 100 km and x = 200 km) that will be discussed later.

[9] The models show that subducting slip perpendicular (θ = 0°) or nearly perpendicular (20°) to the trench axis can cause an increase in the static Coulomb stress on strike-slip faults located far away from the trench, but a decrease in the Coulomb stress on strike-slip faults near the trench axis (Figures 2a and 2b). On the other hand, highly oblique (θ = 45°) or trench axis parallel slip (θ = 90°) on the subduction interface will increase the static stress on strike-slip faults close to the trench but decrease the stress on strike-slip faults far away from the trench and within the forearc (Figures 2c and 2d).

[10] There appears to be a trade-off between slip azimuth and the coefficient of friction in determining the pattern of Coulomb stress change on strike-slip fault planes in the forearc. The pattern predicted from a model with high slip azimuth, θ, and high coefficient of friction, μ, resembles the pattern predicted from lower slip azimuth and lower coefficient of friction. For example, the pattern predicted by a model with θ = 45° and μ = 0.8 (Figure 2e) is similar to the pattern by a model with θ = 20° and μ = 0.4 (Figure 2b). Likewise, the pattern predicted by a model with θ = 20° and μ = 0.1 (Figure 2f) resembles the pattern by a model with θ = 45° and μ = 0.4 (Figure 2c).

[11] The models therefore indicate that to a first order, slip on the subduction zone induces a bimodal pattern of stress change on nearby strike-slip faults in the forearc region (Figure 2). This pattern depends on the slip azimuth of the subduction earthquake and on the coefficient of friction. The bimodal pattern is apparent in Figure 3, which shows contours of average Coulomb stress change on the strike-slip fault as a function of slip azimuth and distance from the trench. The average Coulomb stress is the mean of the Coulomb stress changes calculated over the strike-slip fault segment between x = 100 and x = 200 km and between the surface and the depth of intersection with the subduction interface. When slip direction is close to perpendicular to the trench axis or forearc faults have a high coefficient of friction, static Coulomb stress is calculated to increase on strike-slip faults that are far from the trench but decrease on strike-slip faults close to the trench. Conversely, when the slip direction is highly oblique to the trench axis or the faults have low coefficient of friction, static stress is calculated to increase on strike-slip faults close to the trench, and decrease on those farther away (Figure 3). The pattern is similar for different slab dips (Figure 3b).

[12] To further understand the reasons for the changing pattern of the induced stresses, we plot the average change of the normal and shear components of the Coulomb stress over the fault segment between x = 100 and x = 200 km and between the surface and the depth of intersection with the subduction interface (Figure 4). The induced normal stress ($\Delta\sigma_n$) is close to zero (unchanged) when the subduction slip is parallel to the trench (θ = 90°) (Figure 4a). For all other cases, when slip is oblique or perpendicular to the trench axis, the calculated average normal stress is positive on

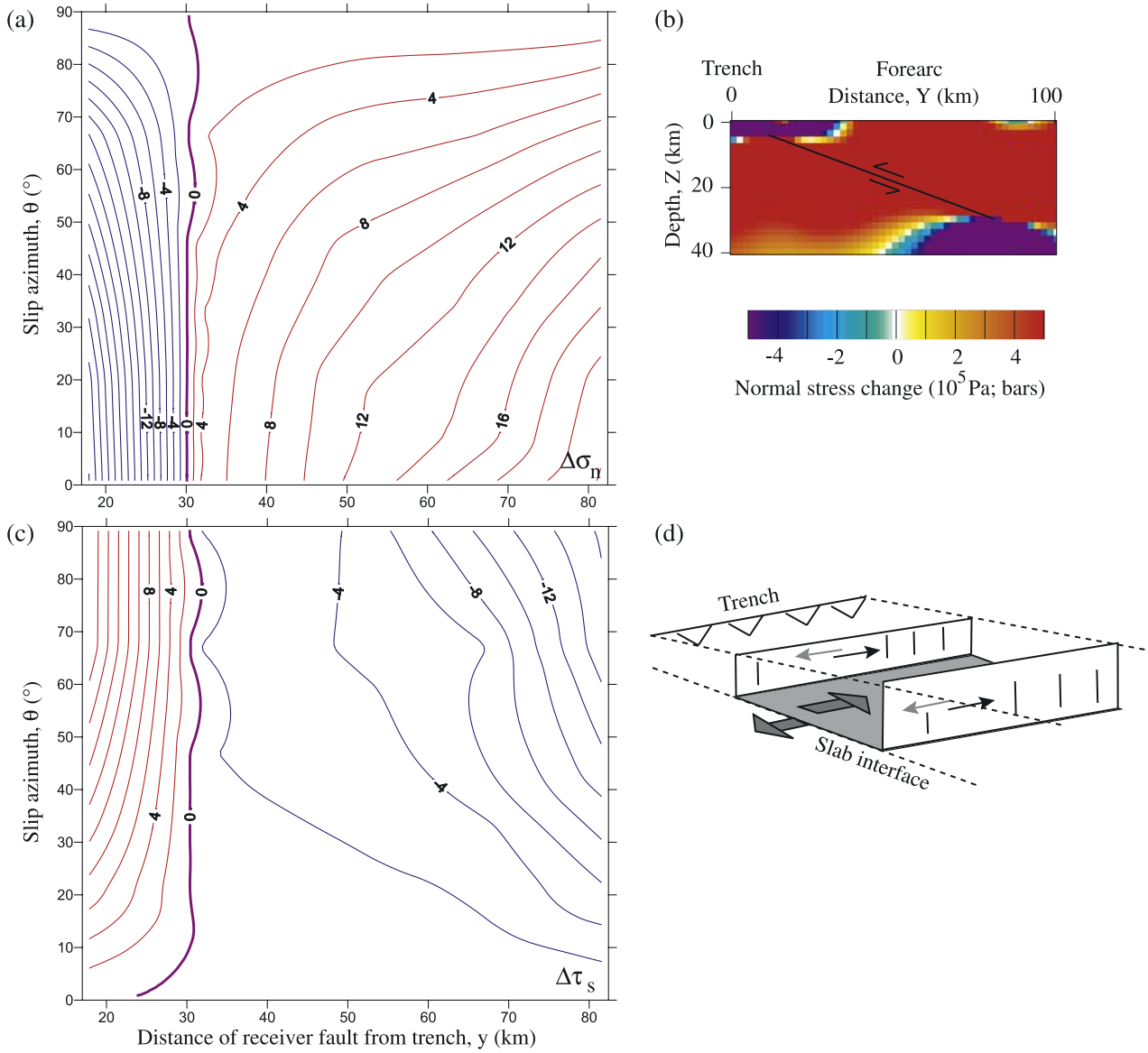

Figure 4. Contours of the average (a) normal ($\Delta\sigma_n$) and (c) shear ($\Delta\tau_s$) stress changes on a strike-slip fault on the forearc as a function of subduction slip azimuth, θ, and the distance, y, of the fault from the trench. The subduction patch is dipping at 20°. (b) Change in normal stress on fault planes that are oriented parallel to the trench due to pure thrust (θ = 0°). Cross section is located at the center of the slipping patch (x = 150 km in Figure 2) and is perpendicular to the trench. (d) Schematic diagram of a rectangular subduction patch with a slip component parallel to the trench (θ = 90°) and left-lateral strike-slip faults intersecting its top and bottom. Note that slip on the patch will promote shear stress on the fault near the trench and unload the shear stress on the fault far from the trench.

faults away from the trench and negative on faults near the trench. In other words, strike-slip faults far from the trench will be unclamped by perpendicular or oblique slip on the subduction interface, whereas strike-slip faults near the trench will be clamped. This is because the rock volume above the subduction interface moves toward the trench during a subduction earthquake, compressing the frontal part of the volume and extending the trailing part of the volume (Figure 4b).

[13] The magnitude of the average shear stress change ($\Delta\tau_s$) is largest for slip parallel to the trench axis and is zero for slip perpendicular to the trench (Figure 4c). In general, and especially in the case of high values of slip azimuth, the average shear stress increases on strike-slip faults close to the trench and decreases on strike-slip faults farther from the trench. This is a consequence of the geometric configuration of the subduction system (Figure 4d). Thrust slip on the subduction patch promotes left-lateral shearing on faults near the trench and right-lateral shearing on faults farther away (Figure 4d).

[14] The components of Coulomb stress calculated for the middepth of the strike-slip faults are shown in Figure 5 as a function of distance along the fault plane. The stress components on the fault intersecting the top end of the

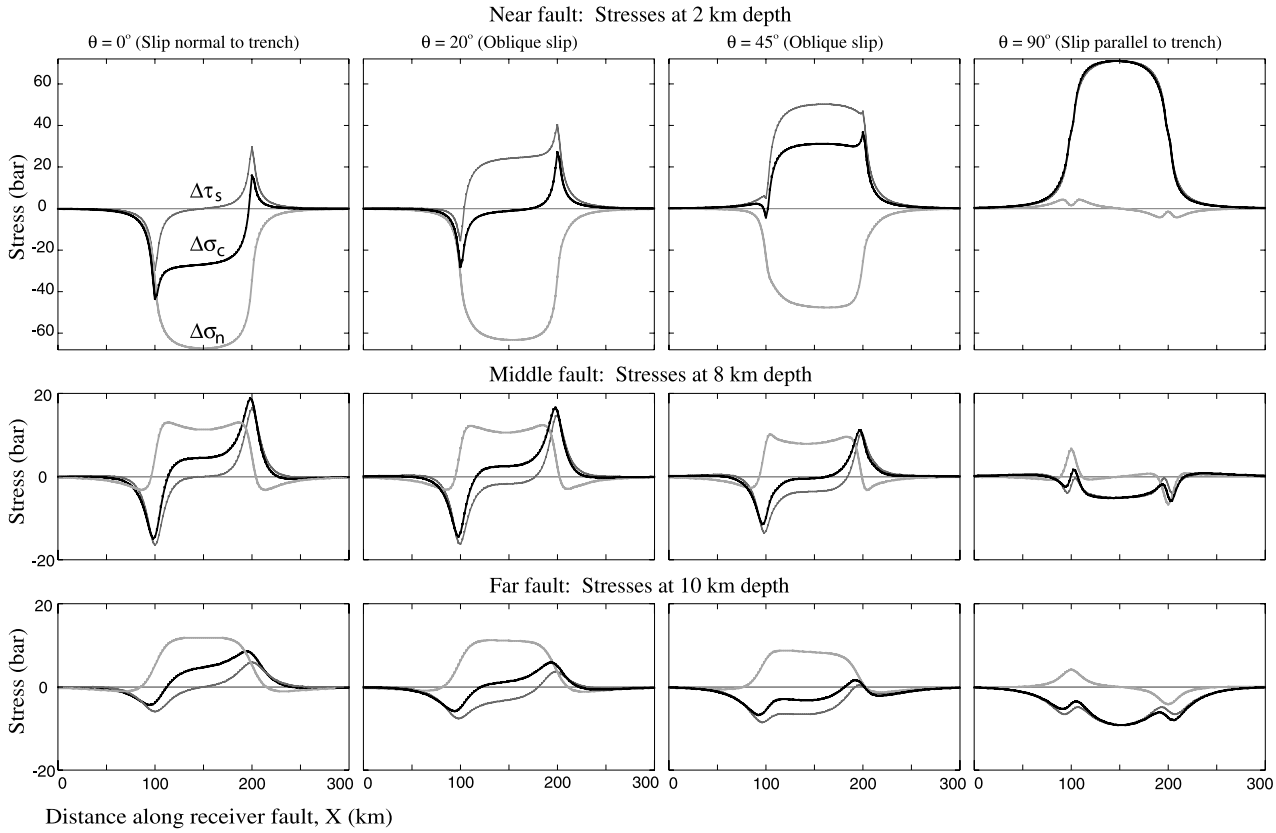

Figure 5. Components of the Coulomb stress change plotted at a specified depth along each fault in Figure 2. The components are shear stress $\Delta\tau_s$ (gray), normal stress $\Delta\sigma_n$ (light grey) and Coulomb stress $\Delta\sigma_c$ (black). Stresses were calculated at depths of 2, 8, and 10 km along faults intersecting the top, middle, and bottom of the patch, respectively, where the intersection depths are 5, 18, and 30 km, respectively. Note change in vertical scale between the top row and the bottom two rows.

thrust is sampled at a depth of 2 km, because the fault intersects the thrust patch at a depth of 5 km. We sampled the stress components on the fault intersecting the bottom end of the thrust at a depth of 10 km, because that is probably close to the nucleation depth of strike-slip earthquakes. Note that the normal stress ($\Delta\sigma_n$) is symmetric with respect to the center of the patch (x = 150 km), whereas the shear stress ($\Delta\tau_s$) is antisymmetric. Therefore Coulomb stress ($\Delta\sigma_c$) is also antisymmetric with respect to the center of the strike-slip fault, giving rise to a positive stress change on one lateral edge of the patch, and a negative stress change on the other lateral edge (e.g., Figure 2b, middle). However, because the positive and negative changes in shear stress have similar amplitude (e.g., $\Delta\tau_s$ in Figure 5 for $\theta = 0$, Near fault), the average shear stress cancels the effects of the lateral edges and is indicative of the stress change in the middle of the strike-slip fault patch.

[15] Coulomb stress ($\Delta\sigma_c$) is simply the sum of shear stress ($\Delta\tau_s$) and the normal stress ($\Delta\sigma_n$) multiplied by a coefficient μ whose value is less than 1. In cases of oblique slip, i.e., high slip azimuth θ, the calculated average shear and normal stresses have opposite signs (Figure 4), so their sum can be either positive or negative. The sign of the calculated Coulomb stress change ($\Delta\sigma_c$) is therefore sensitive to the choice of the coefficient of friction μ, as shown in Figures 2e and 2f.

[16] The subduction patch in our analysis has along-trench length to downdip width ratio of 1.37, which is sufficiently large to isolate the changes that occur in the middle of the trench parallel strike-slip faults (Figure 5). Although many moderate-size thrust earthquakes have a similar or smaller length/width ratio, large subduction earthquakes have aspect ratios between 2 and 6.5 [*Lin and Stein*, 2004]. Doubling the aspect ratio of the subducting patch, as shown in Figure 6, stretches the stress pattern in the central part of the patch, but the resultant stress pattern is otherwise similar to that for a ratio of 1.37.

[17] The above analysis illustrates two contributions of equal importance to the calculated Coulomb stress changes on strike-slip faults in the forearc region: Changes in normal stress (clamping or unclamping) on these faults and changes in the shear stress. The assumed coefficient of friction on the faults affects the magnitude and sign of the Coulomb stress change by modifying the contribution of the normal stress changes. In general increasing slip azimuth, θ, raises the calculated shear stress on strike-slip faults close to the trench but decreases the shear stress on strike-slip faults farther away (Figure 4).

3. Northern Caribbean Plate Boundary

[18] The contrasting styles of forearc deformation in two segments of the Northern Caribbean trench are next

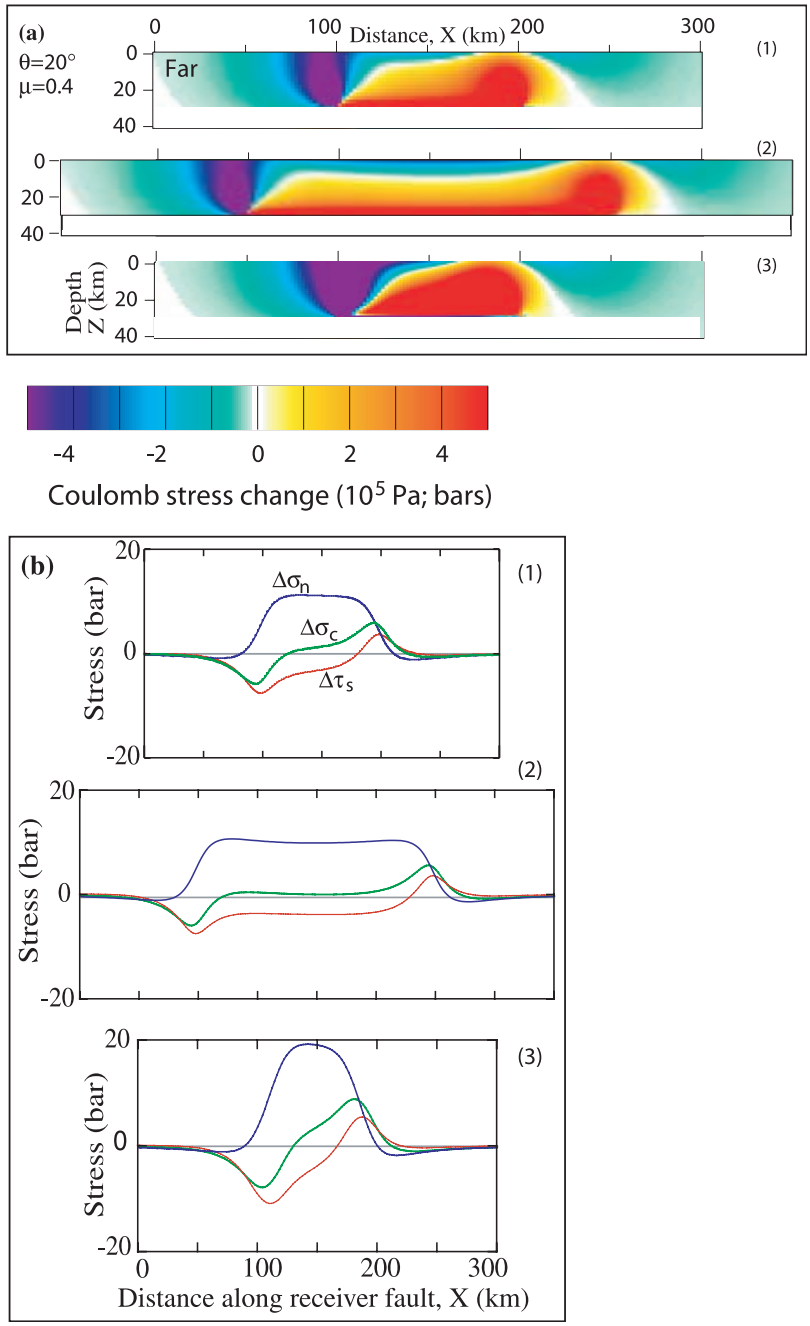

Figure 6. Effects of a larger length/width aspect ratio and a nonuniform slip on the subduction slip. (a) Coulomb stress changes along a fault plane intersecting the patch far from the trench, for slip orientation ($\theta = 20°$ calculated with a coefficient of friction $\mu = 0.4$). Only the portion of the fault plane above the subduction patch is shown. Figure 6a, fault 1, is similar to Figure 2b, far fault. Figure 6a, fault 2, is similar to Figure 6a, fault 1, except with double the length of the subduction patch (200 km). Figure 6a, fault 3, is similar to Figure 6a, fault 1, except with a slip tapered to zero at the edges of the patch starting at a distance equal to 0.2 the length and the width of the patch. (b) Components of the Coulomb stress change plotted at a 10 km depth along each fault (1, 2, and 3) in Figure 6a. The components are shear stress $\Delta\tau_s$ (red), normal stress $\Delta\sigma_n$ (blue), and Coulomb stress $\Delta\sigma_c$ (green).

interpreted in light of the model results. We first review and interpret the deformation in these segments using GPS results, earthquake focal mechanisms, and seafloor topography.

[19] The Greater Antilles volcanic arc, which extends from Cuba to the Virgin Islands, was formed during the Cretaceous and early Tertiary as the NOAM plate was subducting southwesterly beneath the Caribbean plate [*Pindell and Barrett*, 1990]. Beginning at 49 Ma, relative plate motion changed to a more easterly direction (~250°), resulting in a more oblique subduction, a large component of left-lateral strike slip, and the cessation of

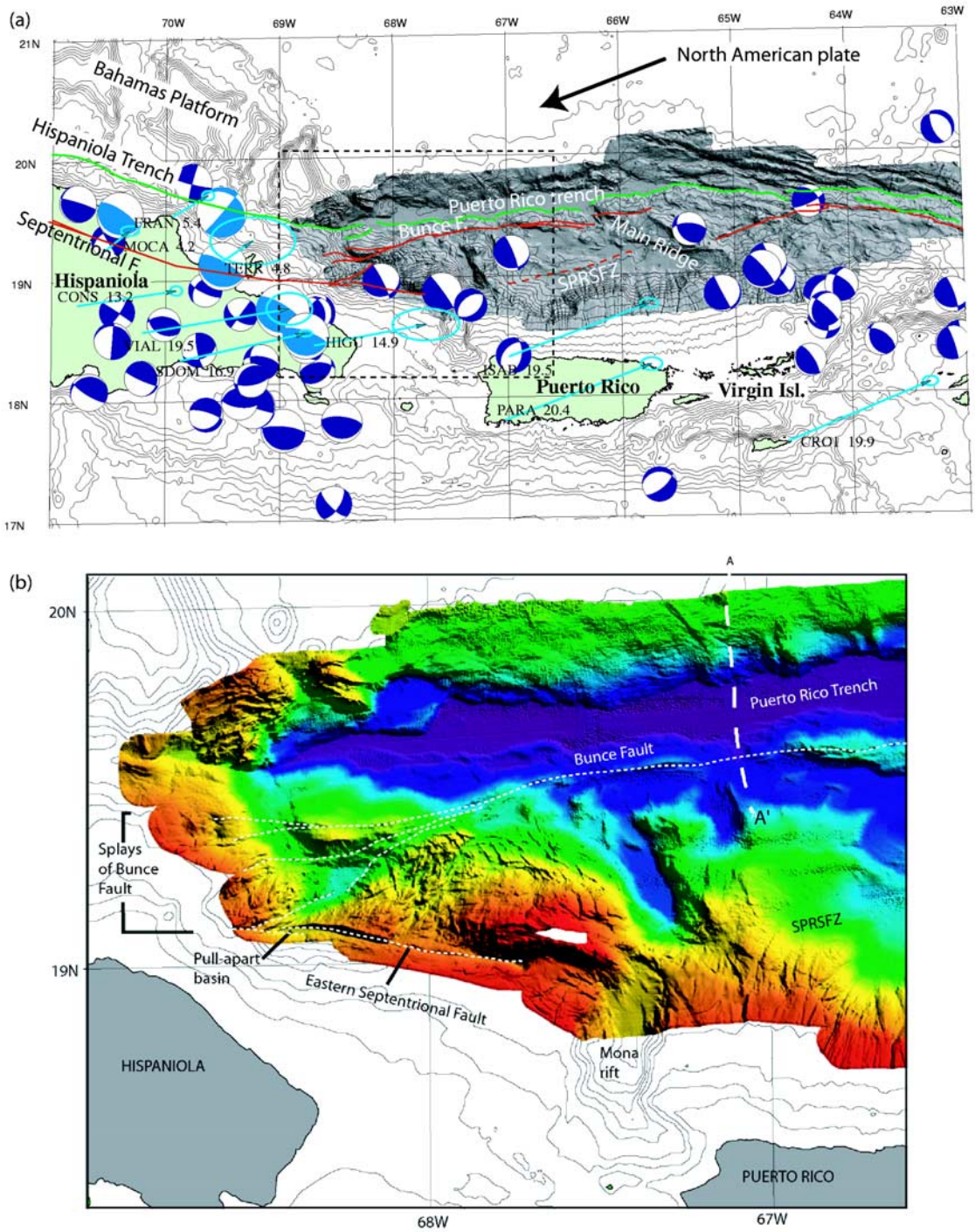

Figure 7. (a) Bathymetry map of the northern Caribbean with a shaded relief map obtained from recent detailed multibeam bathymetry survey [*ten Brink et al.*, 2004]. Dashed rectangle indicates location of enlargement (Figure 7b). Solid green line indicates frontal thrust of the subduction zone. Solid red line indicates interpreted strike-slip faults. Blue beach balls indicate focal plane solutions (lower hemisphere) of moderate earthquakes between 1977 and 2002 from the Harvard CMT catalog. Light blue beach balls indicate same for historical earthquake sequence (D. Wald, personal communication, 2003). Blue lines with ellipses at their ends indicate velocity vectors relative to stable North America accompanied by rate (in mm/yr) and station name, and error ellipse [after *Calais et al.*, 2002]. (b) Enlargement of the bathymetry map near the western end of the Puerto Rico trench, where the Bunce and Septentrional faults overlap. Note the abrupt eastward termination of the Septentrional Fault in a hole. Dashed line A–A′ is location of seismic profile in Figure 8.

arc volcanism. This relative plate motion has been fairly stable ever since as evident from the opening of Cayman Trough between Cuba and Honduras ([*ten Brink et al.*, 2002] and references therein). Presently, a typical old oceanic crust of ~120 Ma in age subducts under Puerto Rico and the Virgin Islands, whereas the descending plate adjacent to the Hispaniola trench is a thick crust of an unknown origin, which underlies the Bahamas platform [*Freeman-Lynde and Ryan*, 1987]. Thrust earthquakes at a shallow angle (20°) under northern Hispaniola [*Dolan and Wald*, 1998] indicate that subduction process is likely to be active there.

[20] According to GPS measurements, slightly oblique convergence under Hispaniola is partitioned between 5.2 ± 2 mm/yr of reverse motion on the subduction interface and 12.8 ± 2.5 mm/yr and 9.0 ± 9.0 mm/yr left-lateral strike slip on the Septentrional and Enriquillo Faults, respectively [*Calais et al.*, 2002] (Figure 7a, Enriquillo Fault is located along the southwest side of Hispaniola beyond the map). The Septentrional Fault, which is a left-lateral strike-slip fault subparallel to the Hispaniola Trench in northern Hispaniola, was last active 770–960 years ago [*Tuttle et al.*, 2003] and is thought to be currently in the late part of its seismic cycle [*Calais et al.*, 2002]. The fault runs along the highly populated Cibao valley and is capable of producing an earthquake of M_w = 7.7–7.9 [*Calais et al.*, 2002]. A series of M_s = 7.0–8.1 earthquakes with mostly thrust motion took place in the eastern half of the Northern Hispaniola between 1946 and 1953 [*Kelleher et al.*, 1973], presumably on the shallow dipping (~20°) subduction interface [*Dolan and Wald*, 1998] (Figure 7). Slip in these events was slightly oblique with average slip azimuth, θ, of 23° (D. Wald, personal communication, 2003). One of these events in 1946 was accompanied by a tsunami, which was rumored to have killed 1500 people [*ten Brink et al.*, 1999]. However, these earthquakes did not trigger seismic activity on the Septentrional Fault.

[21] The forearc region of the Puerto Rico trench appears to be deforming differently than that of Hispaniola. GPS measurements indicate that, contrary to Hispaniola, oblique convergence is not partitioned here. The velocity vector of Puerto Rico relative to the NOAM plate is similar, within measurement uncertainties, to that of the Caribbean plate relative to NOAM [*Calais et al.*, 2002; *Mann et al.*, 2002]. These measurements also do not show significant internal deformation within Puerto Rico itself as evident, for example, from comparing stations PARA and ISAB in Figure 7a. With the exception of the 1943 M_s = 7.3 earthquake northwest of Puerto Rico (Figure 7a), no large instrumentally recorded earthquakes in Puerto Rico can be related with certainty to the subduction interface, although widespread damage in Puerto Rico in 1787 led *McCann et al.* [2004] to propose a magnitude 8 earthquake north of the island. The 1943 earthquake had a relatively large slip azimuth, θ = 50° with respect to the trench (D. Wald, personal communication, 2003). Focal mechanisms for seven events of magnitude M_w = 5.3–6.0 (Harvard CMT) show a highly oblique slip azimuth (θ = 67° on average) that is subparallel to the plate motion vector. All the events have shallow dipping angle of ~20°.

[22] The geometry of strike-slip faults in the Puerto Rico forearc region is not well known because the area is largely submerged. Various authors [*van Gestel et al.*, 1998; *Muszala et al.*, 1999] proposed that the Septentrional Fault continues eastward from Hispaniola along the shelf slope north of Puerto Rico to become the South Puerto Rico Slope Fault Zone (SPRSFZ). Others [*Masson and Scanlon*, 1991; *Dolan et al.*, 1998; *Mann et al.*, 2002] instead proposed that a strike-slip fault, called the North Puerto Rico Slope Fault Zone (NPRSFZ), lies close to and parallel to the trench axis. The connection between this fault and the Septentrional Fault in Hispaniola was not clear.

[23] A new multibeam bathymetry map of the Puerto Rico trench (Figures 7a and 7b) reveals the active fault geometry of the Puerto Rico and Virgin Islands forearc. The map shows a continuous fresh fault scarp 10–15 km south of the trench. Part of this fault coincides with the NPRSFZ that was previously noted on low-resolution Gloria side-scan sonar data. However, its definition, detailed features, and lateral extent are much better defined by the new multibeam bathymetry data. The fault extends over 535 km from northeast of Hispaniola to the northern end of the Lesser Antilles and is disrupted only by a subducted seamount known as Main Ridge (Figure 7a). We name this fault the Bunce Fault in honor of Dr. Elizabeth Bunce, a pioneer marine geophysicist who worked on the science of the Puerto Rico trench in the 1950s. The slip on the Bunce Fault is probably left lateral, because a small deep basin (8,300 m deep) at longitude 66.2°W is interpreted to be a pull-apart basin formed by left-lateral motion across a left step in the fault. A vertical discontinuity separating sections of different reflectivity on either side can be seen on a seismic reflection profile across the Bunce Fault (Figure 8). The fault extends down to the subduction interface about 5 km deep. The morphological character of the hills along the Bunce Fault suggests that it cuts through accretionary prism sediments.

[24] The new bathymetry data show no clear continuous fault trace of the previously hypothesized extension of Septentrional Fault beyond Mona rift along the SPRSFZ (Figure 7b). Intermittent E-W and ENE-WSW oriented lineaments (Figure 7b) may attest to old fault configuration that is no longer active.

4. Stress Interaction and Deformation of the Northern Caribbean Forearc Region

[25] An unusual relationship is observed between the Septentrional and Bunce strike-slip faults. This relationship may reflect changes in the slip azimuth of subducting slabs between the Hispaniola and Puerto Rico segments of the subduction zone. The Bunce Fault runs close to the Puerto Rico trench throughout its length, but turns southward and away from trench as the Hispaniola trench is approached (Figure 7b). There, the fault splays into several strands presumably to accommodate a more diffuse deformation over a larger area. Although one of these strands reaches the Septentrional Fault, it is unlikely that left-lateral motion is transferred from one fault to the other along this strand. If this were the case, then a large pull-apart basin would have been opened between the two faults as would be required by the geometry of left offset in a left-lateral system. Instead, the Septentrional Fault continues eastward overlapping with the Bunce Fault for about 80 km. The morphology of the Septentrional Fault at the area of overlap indicates

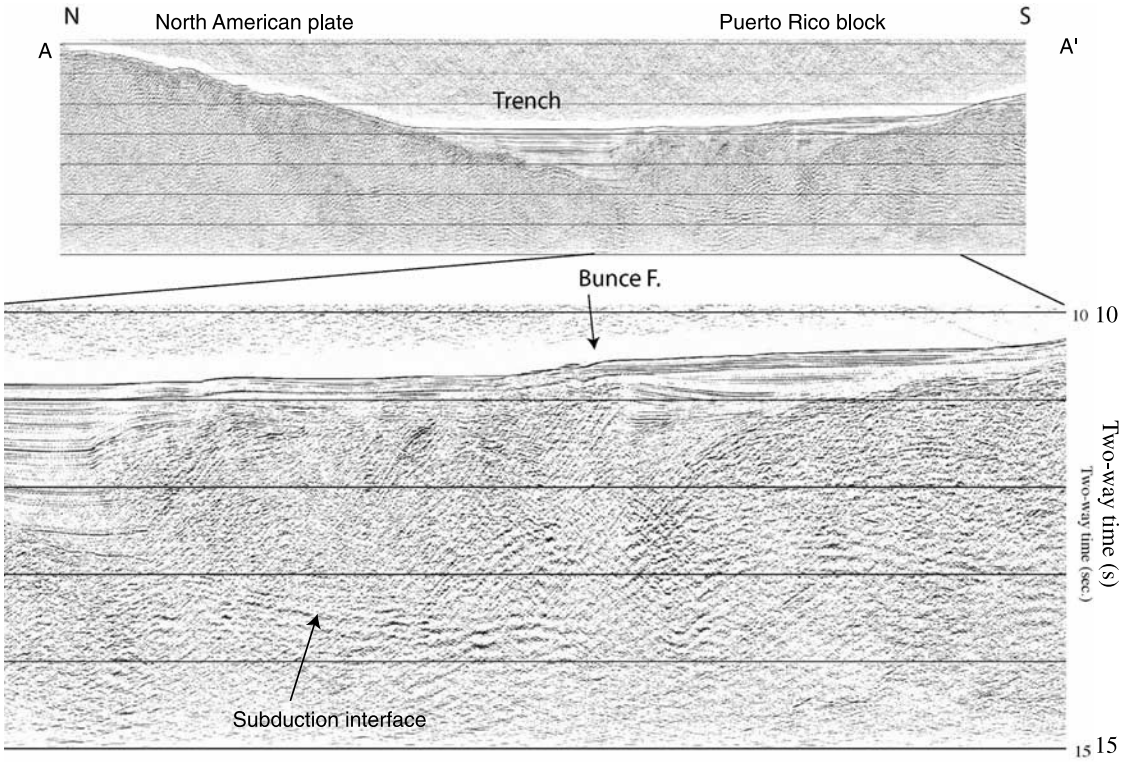

Figure 8. Migrated seismic profile NAT44 across Bunce Fault showing that the fault is vertical and terminates at shallow (~5 km) depth against the subduction interface. See Figure 7b for location.

an active left-lateral slip because a small pull-apart basin was observed (Figure 7b). The Septentrional Fault is bounded by a 1,500 m scarp, follows a linear depression, and finally terminates abruptly 20 km west of the Mona rift in a circular depression several hundreds meters deep. Mona rift is a site of active east-west extension within the forearc region (Figure 7b).

[26] We interpret the observed change in the location of the strike-slip fault system, from the interior of the forearc region in the Hispaniola segment, to the vicinity of the trench in the Puerto Rico segment to reflect changes in the slip direction on the down-going slab in these two segments. According to our calculations, the relatively small slip azimuth of the Hispaniola segment earthquakes ($\theta = 22^\circ$) causes an increase of the static Coulomb stress on strike-slip faults in the back of the forearc region far away from the trench (Figure 3a). In contrast, the slip azimuth on the Puerto Rico segment is highly oblique ($\theta = 67^\circ$), and thus Coulomb stress is predicted to increase on faults near the trench (Figure 3a).

[27] We calculate the Coulomb stress change more accurately on the actual mapped or hypothesized strike-slip fault strands in the Hispaniola and Puerto Rico forearc regions (Figure 9). In Figure 9a, the stress change is caused by slip on a 304 km x 102 km section of the slab, which extends from depth of 5 km to 40 km at a dip angle of 20° under the Puerto Rico trench segment. Because of lack of large earthquakes in this segment, we use the average slip parameters from the Harvard CMT catalog for moderate ($M = 5.3–6.0$) earthquakes in the past 25 years to define the model slip parameters. A slip magnitude of 2 m is used, which corresponds to ~100 years of the average plate convergence based on the convergence rate from GPS measurements. This slip should be considered a proxy for the secular motion on the Puerto Rico subduction interface. In Figure 9b, the stress change is caused by slip on a 180 km × 117 km patch of the slab under Hispaniola that extends from depth of 0 km to 40 km at a dip angle of 20°. The size of the patch corresponds to the area that was ruptured during the 1946–1953 series of earthquakes [*Dolan and Wald*, 1998]. Slip parameters are taken to be the average slip parameters of the thrust events in the 1946–1953 earthquake series (D. Wald, personal communication, 2003). Secular motion can be added to the calculated Coulomb stress change for these earthquakes, by adding the pattern of Figure 9a, to that of Figure 9b. We do not consider secular slip to happen at a depth >40 km on the Hispaniola patch of the slab, because at this depth the slab is located within the upper mantle.

[28] The calculated Coulomb stress increases on the Bunce Fault and on two out of its three main splays because of the highly oblique slip in the Puerto Rico trench (Figure 9a). The calculated Coulomb stress decreases on the SPRSFZ, a previously hypothesized continuation of the Septentrional Fault, also due to oblique slip in the Puerto Rico trench. The SPRSFZ falls within the quadrant of decreased average Coulomb stress in our generic model, because of its larger distance from the trench (Figure 3a).

[29] Coulomb stress increases in the central segments of the Septentrional Fault, resulting from the combined effect of slip on the Hispaniola patch (Figure 9b) and the oblique secular motion on the Puerto Rico patch (Figure 9a). Coulomb stress decreases on the part of the Septentrional Fault close to the western edge of the Hispaniola patch but

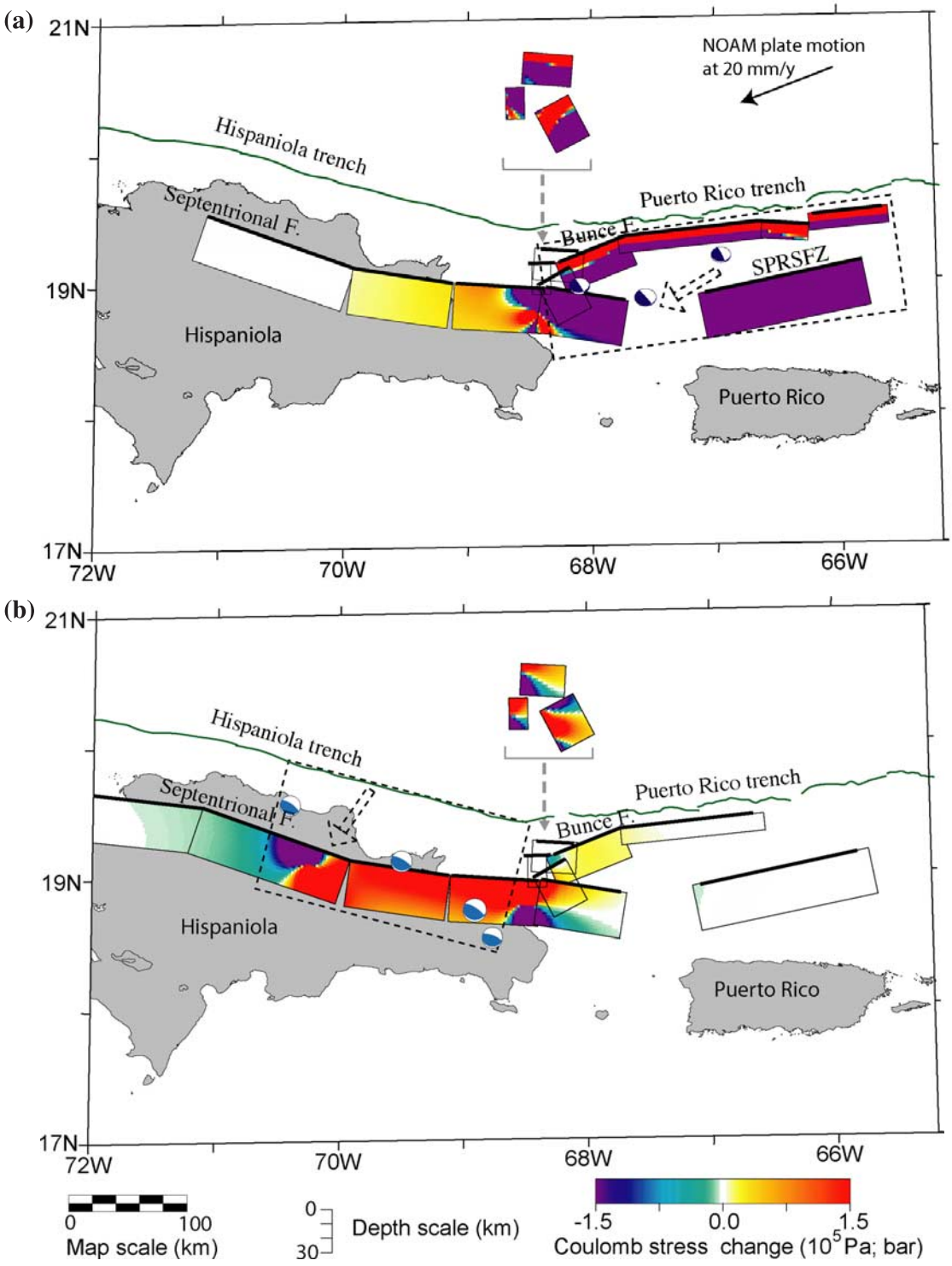

Figure 9. Static stress change models for known or hypothesized faults in the Hispaniola and Puerto Rico subduction segments (shown in Figure 7) due to (a) slip on a patch of the Puerto Rico subduction zone and (b) slip on a patch of the Hispaniola subduction zone. The open dashed arrow denotes slip direction, and the patches are marked by dashed rectangles. Heavy black lines are simplified fault traces. Colored rectangles below the fault traces represent the Coulomb stress change on vertical fault planes associated with these fault traces assuming left-lateral strike-slip motion on the fault planes. Earthquakes used to determine average slip parameters are shown as beach balls.

increases close to the eastern edge of the patch. This antisymmetric pattern at the lateral edges of the strike-slip fault patch within the forearc region is predicted by the generic models (e.g., Figure 2b) and is due to the antisymmetric pattern of the shear stress component (Figure 5). It is expected that the western part of the Septentrional Fault, which is associated with negative Coulomb stress, will become positive should a thrust earthquake occur on the subducting slab west of the present patch.

[30] On the eastern end of the Septentrional Fault, which overlaps with the Bunce Fault, the Coulomb stress is calculated to increase from thrusting in the Hispaniola trench (Figure 9b), but to decrease from oblique secular motion in the Puerto Rico trench (Figure 9a). Therefore the resultant Coulomb stress is expected to reverse its sign during an earthquake cycle. In summary, static stress due to thrust motion on the northern Caribbean slab is calculated to increase along major portions of the Septentrional and Bunce Faults, which are the known active strike-slip faults in the Caribbean forearc region, but to decrease on SPRSFZ, which is inferred to be inactive from our bathymetry data.

5. Discussion

[31] Our modeling results are in qualitative agreement with the modeling results of *Taylor et al.* [1998]; however, we focus on the predicted stress changes in the forearc region above the subduction patch, whereas *Taylor et al.* [1998] focused their discussion specifically on explaining several back-arc earthquakes in the Aleutian and Irian Java subduction zones following large oblique subduction earthquakes. We present a range of generic models that cover the spectrum of slip azimuths and location of the forearc strike-slip receiver faults, as well as illustrate the shear and normal stress components in each model to better understand the contributions of each component to the Coulomb stress change. *Taylor et al.* [1998] plotted stress changes near the surface of the upper plate, whereas stresses can vary with depth (e.g., Figure 2b) and earthquakes generally nucleate at depth. For simplicity, we ignore the stress change concentrations near the edges of the slipping patch in our discussion, although they can be locally significant. As *Taylor et al.* [1998] have shown, these stress change concentration can explain the concentration of specific arc and back-arc earthquakes in relation to earthquake slip on the subduction interface.

[32] A uniform slip over the entire subduction patch is modeled here for simplicity, although in reality the slip can be spatially variable. Such variable slip is likely to have some effects on the pattern of the resultant Coulomb stress changes. For example, linearly tapered slip distribution along both the strike and downdip directions of a subduction patch results in a more gradual change of Coulomb stress between the two lateral edges of the strike-slip fault, in comparison to the results of the uniform slip case (Figure 6). The Coulomb stress change pattern may also be further complicated by afterslip motion on the subduction interface downdip or updip from the patch that slipped during an earthquake. The effects of spatially variable slip and of afterslip can be calculated by linear superposition.

[33] A particularly illuminating aspect of our generic models is the contribution of slip on subduction interface to the change in normal stresses on the trench-parallel strike-slip faults in the forearc region. Both perpendicular and oblique thrust motions on the subduction interface make the normal stress more positive (unclamping) on trench-parallel strike-slip faults that are farther away from the trench. On the other hand, normal stress becomes more negative on strike-slip faults near the trench, which clamps the faults and inhibits failure (Figures 4a and 5). The increase in normal stress (the unclamping effect) facilitates failure and sliding on fault planes farther away from the trench. *Pollitz and Sacks* [1997] proposed that the reduction in normal stress following two major subduction zone earthquakes in Nankai Trough, Japan, contributed to the failure of the Nojima Fault during the 1995 Kobe strike-slip earthquake. Changes in normal stress will affect all trench-parallel strike-slip faults in the forearc and not only those that have left-lateral motion. The planes to be affected by changes in normal stress do not even have to be faults. For example, thrust slip at the base of a volcano, such as happened southeast of Kilauea, Hawaii, will aid in opening dikes and rifts near the summit of the volcano. The unclamping effect of subduction zone slip may induce landslides because positive change in normal stress may help overcome rock cohesion. Therefore a low-angle thrust earthquake on the subduction interface can have large seismic, volcanic, or tsunamogenic impacts on the overlying forearc or volcano.

[34] The above models underscore the important effect of slip on the subduction interface on deformation of the forearc region, in particular, the dependence of the Coulomb stress change in the forearc on slip azimuth on the subduction patch. Unlike the normal stress, shear stress increases with slip azimuth on strike-slip faults that are close to the trench but decreases on faults that are farther away from the trench (Figures 4c and 5). Thus the effect of slip azimuth on strike-slip faults in the forearc region is more complicated than the predicted effect by kinematic models.

5.1. Relationship to Long-Term Deformation of the Forearc Region

[35] Our elastic models examine the static stress changes immediately after a slip event, in the form of either an earthquake or a creeping event, has occurred on the subduction interface. Subduction zones undergo cycles of strain accumulation (interseismic) and release (coseismic) that are superimposed on the regional strain field of plate convergence [*Savage*, 1983]. These cycles of changes are observed in the uplift, tilt, and horizontal strain of the forearc region overlying the subduction zone [e.g., *Zheng et al.*, 1996]. Geodetic and tide gage data in Japan indicate, however, that postseismic effects through volumetric viscoelastic relaxation dominate over reloading effects of the subduction interface for at least the first quarter or third of the reloading cycle [*Pollitz and Sacks*, 1997]. It was demonstrated that the incorporation of a relaxing viscous-elastic channel underlying the brittle layer in static stress change models serves to prolong the postseismic effect of subduction earthquakes by about 30–50 years [*Pollitz and Sacks*, 1997]. However, since the viscoelastic effects could be nonlinear [*Freed and Burgmann*, 2004], they diminish with time until they become smaller than the effects of secular strain accumulation and stress reloading on the subduction zone. These loading effects induce stresses that are opposite in sign to

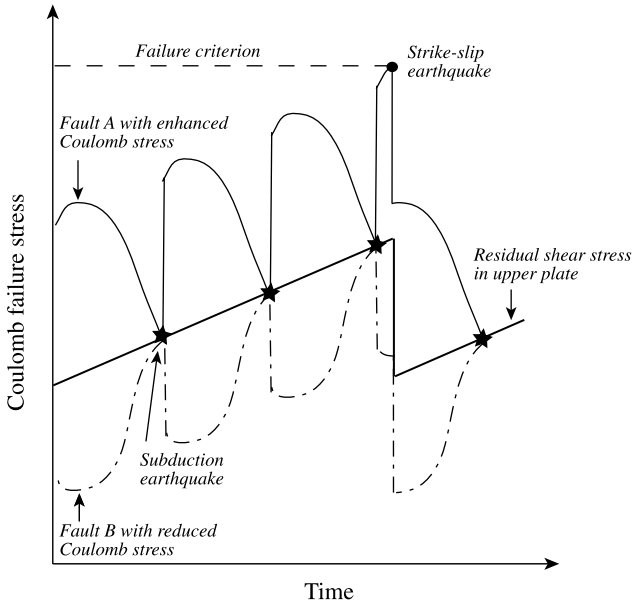

Figure 10. Schematic loading sequence for faults in the forearc due to subduction earthquakes, illustrating the role of transient Coulomb stress changes in strike-slip fault rupture in the forearc. Coseismic stress increase and decrease occur on different faults following a subduction earthquake. These coseismic changes may continue as much as a 1/4 or a 1/3 of the earthquake cycle due to viscoelastic relaxation effects [*Pollitz and Sacks*, 1997] but will eventually decay. This loading sequence is superimposed on a gradual increase in the regional shear stress in the forearc. (The increase may be stepwise after a subduction earthquake if the regional stress is the residual shear component of plate convergence that is released during earthquakes on the subduction interface.) The first fault to rupture is a fault where the superimposed positive Coulomb stress change helps it to reach a failure criterion.

those induced by a slip event on the subduction zone until the next earthquake occurs. However, the reloading effects may not completely reverse the coseismic stress changes, resulting in a gradual increase of the Coulomb stress change over several earthquake cycles [*Pollitz and Sacks*, 1997].

[36] A more fundamental question is whether the deformation pattern of strike-slip faults in the forearc region is governed by the regional stress field or by the short-term perturbations due to subduction thrust events. One source of regional shear stress is the expected deficit in lateral strain along the subduction interface, caused by the difference between slip azimuth and plate convergence azimuth in some subduction zones (Figure 1). If this trench-parallel regional shear stress is capable of deforming the forearc and arc regions independently from the thrust events on the subduction interface, as is some times modeled [e.g., *Robinson and Benites*, 1996], the location of the optimally situated active strike-slip faults will not need to depend on the subduction event-induced Coulomb stress changes discussed here.

[37] We argue that although the subduction event-induced Coulomb stress changes are perturbations on a regional stress field, they nevertheless exert significant influence on the location of the optimally situated strike-slip faults. Figure 10 shows a schematic loading history of the forearc region, in which each subduction earthquake raises the Coulomb stress in the region where hypothetical Fault A is located, and reduces the stress in the region where hypothetical Fault B is located. These subduction event-induced stress perturbations decay during the interseismic period. The regional shear stress builds up with time (either linearly or in steps) because slip on subduction earthquakes does not release the entire trench-parallel component of the regions stress. An earthquake could occur on a strike-slip fault in the forearc region if a local failure criterion is reached. Immediately after a subduction event, Fault A is likely to reach the failure stress level earlier than Fault B because of its elevated Coulomb stress relative to Fault B (Figure 10). Therefore Coulomb stress changes play a significant role in the deformation of the forearc region despite their ephemeral nature.

5.2. Other Forearc Regions

[38] Fault distribution in forearc regions is generally poorly known because these regions are submerged underwater. Only a few other forearc regions are mapped in as much detail as the 800 km long segment of the northeast Caribbean plate [*ten Brink et al.*, 2004]. Detailed bathymetry maps of the southern end of the Ryukyu trench reveal strike-slip faults within the accretionary prism at distances of 35–45 km from the trench [*Lallemand et al.*, 1999]. Convergence direction at this segment of the trench ranges from 40° to 60° off the trench-normal direction [*Lallemand et al.*, 1999]. The dip angle of the seismogenic zone is 10°–15° and the slip azimuth is $\theta = 35° \pm 12°$ [*Kao et al.*, 1998]. A slip azimuth of 35° is at the transition between the trench-perpendicular and trench-parallel modes of thrust on the subduction interface. Figure 3b nevertheless predicts a weak increased Coulomb stress at this distance due to subduction events.

[39] Although oblique subduction in the Sunda trench off Sumatra reaches up to $\theta = 70°$, slip azimuth along the Sumatra segment of the trench is $\theta \leq 25°$ [*McCaffrey*, 1994; *McCaffrey et al.*, 2000]. Detailed bathymetry of the forearc region is lacking but seismic reflection profiles indicate that the closest strike-slip fault to the trench is the Mentawai fault zone located within a forearc basin at distances of 110–150 km from the Sunda trench [*Schlüter et al.*, 2002]. Our models predict that strike-slip faults will be located toward the back of the forearc region, which is in qualitative agreement with the observations.

6. Implications for Seismic and Tsunamogenic Hazard in Puerto Rico and Virgin Islands

[40] GPS measurements and focal plane solutions of earthquakes on the northern Caribbean subduction interface are compatible with the interpretation based on the location of active strike-slip faults in the forearc region, and with predictions of the static stress change models. These observations and the models indicate that slip on the subduction interface of the Puerto Rico segment is highly oblique to the trench axis. Strike-slip faulting appears to be mostly concentrated along the Bunce Fault, which is located more than 100 km north of the northern shore of Puerto Rico. The

Bunce Fault is probably capable of generating only moderate size earthquakes because it extends only down to a depth of 5 km and may rupture partially consolidated accretionary sediments. Focal plane solutions of moderate earthquakes south of the Bunce Fault suggest that slip is subparallel to the relative convergence direction between the North American and Caribbean plates. Static stress change models indicate that thrust events on the Puerto Rico subduction interface should tend to release stress on the SPRSFZ (Figure 9), a fault closer to Puerto Rico, which was previously suggested to be active. Finally, GPS results from Puerto Rico show little, if any, internal deformation across the western end of the island [*Calais et al.*, 2002] (Figure 7a).

[41] On the basis of the above observations and modeling, we thus suggest that the seismic hazard to Puerto Rico and the Virgin Islands from left-lateral strike-slip faults is low. Moreover, the directivity of the oblique thrust events on the subduction interface points in general toward eastern Hispaniola rather than Puerto Rico or the Virgin Islands, thus ground shaking on these islands may not be as severe as if slip was directed at them [e.g., *Gomberg et al.*, 2001]. On the other hand, our generic stress change models suggest some positive change in normal stress in the interior of the forearc region due to thrusting on the subduction interface even when the slip is highly oblique (Figure 4). This may weaken dip-slip faults in Puerto Rico and on its northern slope, and perhaps promote cracking and submarine slides, which are observed along the northern slope [*ten Brink et al.*, 2004].

[42] Our models predict that secular motion on the Puerto Rico segment and thrust earthquakes on the Hispaniola segment will increase Coulomb stress on a significant part of the Septentrional Fault in Hispaniola (Figure 9). The Septentrional Fault last ruptured 770–960 years ago [*Tuttle et al.*, 2003] and is thought to be in the late part of its seismic cycle [*Calais et al.*, 2002]. Thus future subduction events may trigger rupture on this fault. By analogy with the 1995 Kobe earthquake in Japan [*Pollitz and Sacks*, 1997], Coulomb failure stress may have continued to increase on the Septentrional Fault from the 1946–1953 sequence of subduction zone earthquakes, due to viscoelastic effects, and this may shorten the time to next earthquake.

7. Conclusions

[43] The interaction between thrust events on the subduction interface and strike-slip faults within the forearc region is studied using 3-D models of static coulomb stress change. The models show that for high slip azimuth ($\theta > \sim 35^\circ$), Coulomb stress is enhanced on strike-slip faults that are located closer to the trench and is reduced on faults farther inland (Figure 3). In contrast, for lower slip azimuth, Coulomb stress is reduced on strike-slip faults that are located closer to the trench and is enhanced on faults farther away from the trench toward inland. This pattern is independent of the dip of the subduction interface (Figure 3). For slip azimuth between 20° and 45°, the calculated stress changes on the strike-slip faults is sensitive to the assumed coefficient of friction for the strike-slip faults. The pattern may be further complicated by nonuniform slip and by afterslip effects. Globally, strike-slip faults are often located in the back part of the forearc region (>50 km from the trench) or in the arc (e.g., summary by *McCaffrey et al.* [2000]), which can be explained by the fact that two third of the slip on subduction interfaces worldwide is at an angle $\theta \leq 20^\circ$, and only 5% is at angle $\theta \geq 45^\circ$ (Figure 1).

[44] A significant contribution to the Coulomb stress change on strike-slip faults in the forearc region comes from changes in the normal stress due to thrust motion on the subduction interface. This contribution is largest for perpendicular subduction and decreases to zero as slip approaches a direction parallel to the trench. Normal stress change is negative near the trench and positive toward the back part of the forearc region. The change in normal stress effectively unclamps faults located in the forearc, allowing them to slip under lower driving stress. The unclamping affects all the faults in the forearc region, not only those with a left-lateral sense of motion. Unlike normal stress, shear stresses increase in the region close to the trench and decrease toward the back part of the forearc. They diminish in magnitude from a maximum when the slip is parallel to the trench to zero when the slip is perpendicular to the trench.

[45] We argue that although the subduction event-induced Coulomb stress changes are perturbations on the regional stress field, they exert significant influence on the deformation pattern of the forearc region. This is because faults with accumulated positive perturbation reach failure before faults with accumulated negative perturbation.

[46] The Coulomb stress change models were used to explain the contrasting deformation patterns between two adjacent segments of the northern Caribbean trench, where the North American plate subducts under the northern Caribbean plate. The jump from a strike-slip fault that is located only 10–15 km from the trench in the Puerto Rico segment to an inland fault in Hispaniola, which is 60 km away from the trench, is interpreted to reflect the change from oblique slip to a more perpendicular slip on the subduction interfaces of these two segments. Models that consider detailed fault geometry in the study area confirm that slip on the subduction interfaces of the Hispaniola and Puerto Rico segments should increase the Coulomb stress on the Septentrional and Bunce strike-slip faults, respectively. On the other hand, the expected slip on the subduction interface reduces the Coulomb stress on the Southern Puerto Rico Slope Fault Zone (SPRSFZ), which is much closer to Puerto Rico than Bunce Fault and was previously hypothesized to be active [*van Gestel et al.*, 1998; *Muszala et al.*, 1999]. Our new multibeam bathymetry data shows the SPRSFZ fault trace to be inactive (Figure 7).

[47] Seismic hazard to Puerto Rico from earthquakes on the strike-slip faults in the Caribbean forearc region is therefore smaller than previously assumed, because the Bunce Fault, which is an active strike-slip fault near the Puerto Rico segment, is more than 100 km north of the Puerto Rico island. On the other hand, the Septentrional Fault, which runs along the densely populated Cibao Valley, is expected to be active and presents a significant hazard to Hispaniola. Because slip along the Puerto Rico trench is highly oblique ($\theta \sim 70^\circ$), normal stresses on faults in the forearc region are expected to be low, i.e., slip on the subduction interface will not significantly unclamp faults in the forearc. Finally, the directivity of the slip on the

mostly east-west trending strike-slip faults in the northern Caribbean points toward Hispaniola, again suggesting that ground shaking in Puerto Rico will be less severe.

[48] **Acknowledgments.** We are grateful to Ross Stein for providing the Coulomb 2.5 modeling software used in this study. Discussion with Wayne Thatcher and reviews by Ken Hudnut, Bill Dillon, Art McGarr, Associate Editor Kelin Wang, and an anonymous referee, substantially improved the quality of this study. J.L. was supported by the National Science Foundation through grant NSF-EAR0003888. Woods Hole Oceanographic Institution contribution 11108.

References

Anderson, G., B. Aagaard, and K. Hudnut (2003), Fault interactions and large complex earthquakes in the Los Angeles area, *Science*, *302*, 1946–1949.

Beck, M. E., Jr. (1983), On the mechanism of tectonic transport in zones of oblique subduction, *Tectonophysics*, *93*, 1–11.

Calais, E., Y. Mazabraud, B. Mercier de Lépinay, P. Mann, G. Mattioli, and P. Jansma (2002), Strain partitioning and fault slip rates in the northeastern Caribbean from GPS measurements, *Geophys. Res. Lett.*, *29*(18), 1856, doi:10.1029/2002GL015397.

Dolan, J. F., and D. J. Wald (1998), The 1943–1953 north-central Caribbean earthquakes: Active tectonic setting, seismic hazards, and implications for Caribbean-North America plate motions, in *Active Strike-Slip and Collisional Tectonics of the Northern Caribbean Plate Boundary Zone*, edited by J. F. Dolan and P. Mann, *Spec. Pap. Geol. Soc. Am.*, *326*, 143–170.

Dolan, J. F., H. T. Mullins, and D. J. Wald (1998), Active tectonics of the north-central Caribbean: Oblique collision, strain partitioning, and opposing subducted slabs, in *Active Strike-Slip and Collisional Tectonics of the Northern Caribbean Plate Boundary Zone*, edited by J. F. Dolan and P. Mann, *Spec. Pap. Geol. Soc. Am.*, *326*, 1–62.

Fitch, T. J. (1972), Plate convergence, transcurrent faults, and internal deformation adjacent to southeast Asia and the western Pacific, *J. Geophys. Res.*, *77*, 4432–4460.

Freed, A. M., and R. Burgmann (2004), Evidence of power law flow in the Mojave desert mantle, *Nature*, *430*, 548–551, (29 July 2004); doi:10.1038/nature0278.

Freeman-Lynde, R. P., and W. B. F. Ryan (1987), Subsidence history of the Bahama Escarpment and the nature of the crust underlying the Bahamas, *Earth Sci. Planet. Lett.*, *84*, 457–470.

Geist, E. L., and D. W. Scholl (1992), Application of continuum models to deformation of the Aleutian island arc, *J. Geophys. Res.*, *97*, 4953–4967.

Gomberg, J., P. A. Reasenberg, P. Bodin, and R. A. Harris (2001), Earthquake triggering by seismic waves following the Landers and Hector Mine earthquakes, *Nature*, *411*, 462–466.

Kao, H., S. J. Shen, and K.-F. Ma (1998), Transition from oblique subduction to collision; earthquakes in the southernmost Ryukyu Arc-Taiwan region, *J. Geophys. Res.*, *103*, 7211–7229.

Kelleher, J., L. Sykes, and J. Oliver (1973), Possible criteria for predicting earthquake locations and their application to major plate boundaries of the Pacific and the Caribbean, *J. Geophys. Res.*, *78*, 2547–2585.

King, G. C. P., R. S. Stein, and J. Lin (1994), Static stress changes and the triggering of earthquakes, *Bull. Seismol. Soc. Am.*, *84*, 935–953.

Kurushin, R. A., A. Bayasgalan, M. Olziybat, B. Enhtuvshin, P. Molnar, C. Bayarsayhan, K. W. Hudnut, and J. Lin (1997), The surface rupture of the 1957 Gob-Altai, Mongolia, earthquake, *Spec. Pap. Geol. Soc. Am.*, *320*, 143 pp.

Lallemand, S., C.-S. Liu, S. Dominguez, P. Schnuerle, and J. Malavieille (1999), Trench-parallel stretching and folding of forearc basins and lateral migration of the accretionary wedge in the southern Ryukyus: A case of strain partition caused by oblique convergence, *Tectonics*, *18*, 231–247.

Lin, J., and R. S. Stein (2004), Stress triggering in thrust and subduction earthquakes, and stress interaction between the southern San Andreas and nearby thrust and strike-slip faults, *J. Geophys. Res.*, *109*, B02303, doi:10.1029/2003JB002607.

Mann, P., E. Calais, J. Ruegg, C. DeMets, P. E. Jansma, and G. S. Mattioli (2002), Oblique collision in the northeastern Caribbean from GPS measurements and geological observations, *Tectonics*, *21*(6), 1057, doi:10.1029/2001TC001304.

Masson, D. G., and K. M. Scanlon (1991), The neotectonic setting of Puerto Rico, *Geol. Soc. Am. Bull.*, *103*, 144–154.

McCaffrey, R. (1993), On the role of the upper plate in great subduction zone earthquakes, *J. Geophys. Res.*, *98*, 11,953–11,966.

McCaffrey, R. (1994), Global variability in subduction thrust zone-forearc systems, *Pure Appl. Geophys.*, *142*, 173–224.

McCaffrey, R., P. C. Zwick, Y. Bock, L. Prawirodirdjo, J. Genrich, C. W. Stevens, S. S. O. Puntodewo, and C. Subraya (2000), Strain partitioning during oblique convergence in northern Sumatra: Geodetic and seismologic constraints and numerical modeling, *J. Geophys. Res.*, *105*, 28,363–28,376.

McCann, W. R., L. Feldman, and M. McCann (2004), Catalog of felt earthquakes for Puerto Rico and neighbouring islands 1492–1899 with additional information for some 20th century earthquakes, *Tectonophysics*, in press.

Muszala, S. P., N. R. Grindlay, and R. T. Bird (1999), Three-dimensional Euler deconvolution and tectonic interpretation of marine magnetic anomaly data in the Puerto Rico Trench, *J. Geophys. Res.*, *104*, 29,175–29,187.

Pindell, J. L., and S. F. Barrett (1990), Geological evolution of the Caribbean region: A plate tectonic perspective, in *The Geology of North America*, vol. H., *The Caribbean Region*, edited by G. Dengo and J. E. Case, Geol. Soc. of Am., Boulder, Colo.

Pollitz, F. F., and I. S. Sacks (1997), The 1995 Kobe, Japan, earthquake: A long-delayed aftershock of the offshore 1944 Tonankai and 1946 Nankaido earthquakes, *Bull. Seismol. Soc. Am*, *87*, 1–10.

Robinson, R., and R. Benites (1996), Synthetic seismicity models for the Wellington region, New Zealand: Implications for the temporal distribution of large events, *J. Geophys. Res.*, *101*, 27,833–27,844.

Savage, J. C. (1983), A dislocation model of strain accumulation and release at a subduction zone, *J. Geophys. Res.*, *88*, 4984–4996.

Schlüter, H. U., C. Gaedicke, H. A. Roeser, B. Schreckenberger, H. Meyer, C. Reichert, Y. Djajadihardja, and A. Prexl (2002), Tectonic features of the southern Sumatra-western Java forearc of Indonesia, *Tectonics*, *21*(5), 1047, doi:10.1029/2001TC901048.

Stein, R. S. (1999), The role of stress transfer in earthquake occurrence, *Nature*, *402*, 605–609.

Taylor, M. A. J., R. Dmowska, and J. R. Rice (1998), Upper plate stressing and seismicity in the subduction earthquake cycle, *J. Geophys. Res.*, *103*, 24,523–24,542.

ten Brink, U. S., W. P. Dillon, A. Frankel, R. Rodriguez, and C. Mueller (1999), Seismic and tsunami hazards in Puerto Rico and the Virgin Islands, *U.S. Geol. Surv. Open File Rep.*, *99-353*. (available at http://pubs.usgs.gov/openfile/of99-353/)

ten Brink, U. S., D. F. Coleman, and W. P. Dillon (2002), The nature of the crust under Cayman Trough from gravity, *Mar. Pet. Geol.*, *19*, 971–987.

ten Brink, U. S., W. Danforth, C. Polloni, B. Andrews, P. Llanes, S. Smith, C. E. Castel, and T. Uozumi (2004), New seafloor map reveals the structure of the Puerto Rico trench and helps assess earthquake and tsunami hazards in the northeast Caribbean, *Eos Trans. AGU*, *85*, 349–354.

Toda, S., and R. S. Stein (2002), Response of the San Andreas fault to the 1983 Coalinga-Nuñez earthquakes: An application of interaction-based probabilities for Parkfield, *J. Geophys. Res.*, *107*(B6), 2126, doi:10.1029/2001JB000172.

Tuttle, M. P., C. S. Prentice, K. Dyer-Williams, L. R. Pena, and G. Burr (2003), Late Holocene liquefaction features in the Dominican Republic: A powerful tool for earthquake hazard assessment in the northeastern Caribbean, *Bull. Seismol. Soc. Am.*, *93*, 27–46.

van Gestel, J.-P., P. Mann, J. F. Dolan, and N. R. Grindlay (1998), Structure and tectonics of the upper Cenozoic Puerto Rico-Virgin Islands carbonate platform as determined from seismic reflection studies, *J. Geophys. Res.*, *103*, 30,505–30,530.

Wang, K., R. Wells, S. Mazzotti, R. D. Hyndman, and T. Sagiya (2003), A revised dislocation model of interseismic deformation of the Cascadia subduction zone, *J. Geophys. Res.*, *108*(B1), 2026, doi:10.1029/2001JB001227.

Zheng, G., R. Dmowska, and J. R. Rice (1996), Modeling earthquake cycles in the Shumagin subduction segment, Alaska, with seismic and geodetic constraints, *J. Geophys. Res.*, *101*, 8383–8392.

J. Lin, Department of Geology and Geophysics, Woods Hole Oceanographic Institution, Woods Hole, MA 02543, USA.

U. ten Brink, Woods Hole Field Center, U.S. Geological Survey, 384 Woods Hole Road, Woods Hole, MA 02543, USA. (utenbrink@usgs.gov)